Planar time-dependent viscoelastic flow – pulsating flow and effect of elasticity number

Joana M.Malheiro[1], Paulo J.Oliveira[1] and Fernando T.Pinho[2]

[1]Universidade da Beira Interior, Unidade de Materiais Têxteis e Papeleiros, Departamento de Engenharia Electromecânica, Calçada Fonte do Lameiro, 6200-001 Covilhã, Covilhã, Portugal
[2]CEFT Faculdade de Engenharia da Universidade do Porto, Rua Dr.Roberto Frias s/n, 4200-465 Porto, Porto, Portugal
email: joanamouramalheiro@gmail.com[1]

Summary

*In this investigation the evaluation of a viscoelastic flow code under unsteady pulsating flow conditions is under taken. The time-dependent problem considered is simple and its analytical solutions is known; The flow generated by a periodic pressure gradient superimposed on a constant Poiseuille flow between two parallel plates. Results were obtained for Newtonian, Oldroyd-B and UCM models and allowed comparison of the effect of elasticity number (*E*) and viscosity ratio (*β*) variation on the non-Newtonian pulsating flow characteristics. Results were plotted against time and space and conclusions were taken. We observed that the variation of elasticity number affects velocity along time and across the channel, depending also on viscosity ratio. Good agreement between numerical and analytical results were obtained however depending on the conditions of the flow fine meshes were needed.*

Keywords: *time-dependent viscoelastic flows; oscillating flow; elasticity number; viscosity ratio*

1 Introduction

The solution of unsteady viscoelastic flow problems are of great importance not only because many flows of interest occur in variable regimes in particular in bio-engineering applications [1-4] but also due to the tendency of non-Newtonian systems to develop instabilities with time. Due to those facts, a large number of investigations are appearing involving calculations of time-dependent flows of viscoelastic liquids that follow differential and integral constitutive equations, using different methods [5-10]. However, there is a lack of simple test cases capable of evaluating the numerical behaviour of existing codes. Therefore, in continuation of the work preformed by Duarte et al [11], where pulsating flow was studied only at elasticity number equal to 1, this paper presents numerical and analytical results of unsteady viscoelastic pulsating flows for different fluid models at different values of elasticity number.

The numerical simulation code was applied to the pulsating flow that results from the application of a pressure gradient (which varies sinusoidally in time) onto a constant Poiseuille flow between two parallel infinite plates. Numerical results and analytical solutions were obtained for three models (Newtonian, Oldroyd-B and Upper-Convected Maxwell) and were compared for five values of elasticity number, E = 0.01, 0.1, 1, 10 and 100.

Good agreement was obtained between numerical results on fair grids and analytical solutions, especially as the solvent viscosity ratio, β tended to 1. However, for those cases where agreement was not initially found, accurate results could still be obtained when very refined meshes were used. In order to study the effect of elasticity number, E, on non-Newtonian pulsating flows, time steps were reduced as the elasticity number was increased because of the high frequency response expected and observed in other studies. Velocity data were plotted against time (centre line velocity) and space (velocity profile) at different elasticity values, and the corresponding discretization errors were evaluated.

2 Governing equations

Numerical simulations in CFD require the simultaneous solution of three equations: the continuity equation, the momentum equation and a constitutive equation (which represents the rheological behaviour of the fluid). In this section, the governing equations are presented. The equation of conservation of mass and the equation of linear momentum, in the absence of body forces are expressed by the general expressions:

$$\nabla.\mathbf{u} = 0 \quad \text{and} \quad \rho\frac{D\mathbf{u}}{Dt} = -\nabla p + \eta_s\nabla^2\mathbf{u} + \nabla\bullet\boldsymbol{\tau} \tag{1}$$

where **u** is the local velocity vector with components *u* and *v* corresponding to the Cartesian coordinates *x* and *y*, respectively, for a two-dimensional problem, ∇p is the pressure gradient, η_s the solvent viscosity, and $\boldsymbol{\tau}$ the extra elastic stress tensor. The general form of the constitutive equation, for the different models considered can be written as:

$$\lambda \overset{\nabla}{\boldsymbol{\tau}} + f\boldsymbol{\tau} = 2f'\eta_p \mathbf{D} \tag{2}$$

where *f* and *f'* are functions of invariants of $\boldsymbol{\tau}$ that enable to distinguish the different models from each other and take the value $f = f' = 1$ for UCM and Oldroyd-B models, **D** the deformation rate tensor and $\overset{\nabla}{\boldsymbol{\tau}}$ is the upper-convected time derivative of the stress tensor. This equation describes the non-Newtonian nature of the fluid, η_p is the viscosity of the polymeric solute and λ is the relaxation time. Solvent and polymeric viscosities are related as follows:

$$\eta_0 = \eta_s + \eta_p \text{ and } \beta = \frac{\eta_s}{\eta_0} = \frac{\lambda_r}{\lambda} \tag{3}$$

where η_0 is the total zero-shear rate viscosity, λ_r the retardation time of the fluid and β is a parameter that defines the contribution of solvent viscosity, characterizing the elastic nature of fluids. The relaxation time, λ, indicates the magnitude of the elastic nature of the fluid, and as the relaxation time increases so does the fluid elasticity. In Eq.(3), when $\lambda = 0$ the Newtonian constitutive equation is recovered with viscosity η_0. For the UCM fluid the solvent viscosity is zero ($\eta_s = 0 \Leftrightarrow \beta = 0$), meaning that this fluid model has polymeric viscosity contribution only and is therefore devoid of any explicit diffusion term in the momentum equation. On the other hand, the Oldroyd-B model, which has the contribution of both solvent and polymeric viscosities at different ratios ($0 < \beta < 1$) becomes equivalent to a linear combination of UCM and Newtonian models.

For the problem at hand, involving a planar channel flow under fully developed conditions, subjected to a sinusoidal pressure gradient,

$$-\frac{1}{\rho}\frac{dp}{dx} = K_s + K_o \cos(\omega t) \tag{4}$$

the continuity equation is automatically satisfied, the momentum equation reduces to:

$$\rho\frac{\partial u}{\partial t} = -\frac{dp}{dx} + \eta_s \frac{\partial^2 u}{\partial y^2} + \frac{\partial \tau_{xy}}{\partial y} \tag{5}$$

and the constitutive equation for the shear stress becomes:

$$\tau_{xy} + \lambda\frac{\partial \tau_{xy}}{\partial t} = \eta_p \frac{\partial u}{\partial y} \tag{6}$$

In Eq. (4) ρK_o is the amplitude of the oscillating pressure gradient, ω the angular frequency of oscillation corresponding to a period $T = 2\pi/\omega$, and the magnitude of the stationary pressure gradient is ρK_s. No slip boundary conditions are applied at the solid walls placed at $y = \pm h$ where h is half the channel width,

$$u(y = \pm h, t) = 0 \text{, for } t > 0 \tag{7}$$

and the flow is started from quincenst conditions, corresponding to the following initial conditions:

$$u(y, t = 0) = 0 \text{ for } -h \le y \le +h \tag{8}$$

Of course we are mainly interested in the cyclic flow once fully-established in time conditions are attained.

In the following, non-dimensional variables will be employed after scaling time with the period of oscillation ($t \equiv t/T$), lengths with the channel half-width ($y \equiv y/h$), velocities with the average velocity under steady-state conditions ($u \equiv u/\overline{u}_s$, with $\overline{u}_s = \rho K_s h^2/3\eta_0$), and pressure and stresses as $\tau_{xy} \equiv \tau_{xy}/\eta_0\overline{u}_s/h$. With this scaling, the relevant independent dimensionless groups are the elasticity and the Womersley numbers and the pressure-gradient ratio, given respectively by:

$$E = \frac{\lambda\eta_0}{\rho h^2}, \quad \alpha = h\sqrt{\frac{\omega\rho}{\eta_0}} \quad \text{and} \quad \frac{K_o}{K_s} \tag{9}$$

The analytical solution for the velocity is given in Duarte *et al* [11] and will be used to compare with the present numerical results:

$$u_{th}(y,t) = \frac{3}{2}\left(1-y^2\right) + \frac{3K_o}{\alpha^2 K_s}\mathrm{Re}\left\{ i\left[\frac{\cosh(Zy)}{\cosh(Z)} - 1\right]\exp(2\pi i t)\right\} \tag{10}$$

where: $$Z = \alpha\left(i\frac{1+i\alpha^2 E}{1+i\beta\alpha^2 E}\right)^{1/2}.$$

The discretization error is based on the Euclidian norm applied to the axial velocity, evaluated either by integration over the channel cross-section or as a mean value over one period:

$$e(t) = \sqrt{\frac{1}{NY}\sum_i \left(u_{\Delta y}(y_i,t) - u_{th}(y_i,t)\right)^2} \quad \text{or} \quad e = \frac{1}{N_t}\sum_{period} e(t) \tag{11}$$

where $u_{\Delta y}$ is the numerical solution on a mesh with *NY* control volumes and mesh spacing $\Delta y = 1/NY$ and N_t is the total number of time steps in a period.

3 Numerical method

A fully implicit finite-volume method was used for the calculation of present one-dimensional time-depend flow whose fluids that follows differential viscoelastic constitutive models. The governing equation presented above are integrated in space over the control volume, forming the computational mesh, and in time over small steps, Δt, in order to obtain sets of linearized algebraic equations. The spatial integration is based on Central Difference Scheme and the temporal integration on the Three-Time Level method. Both schemes are second-order accurate and are applied on a non-staggered grid arrangement (mesh type B), with uniform spacing in *y* direction, Δy, and in which all dependent variables are located at the centre of the control volumes. The linearized algebraic equations and for the stress of motion to be solved for $\phi = u$ or τ_{xy}. Here will be in its simplified form expressed as:

$$a_P\phi_P^{n+1} = a_N\phi_N^{n+1} + a_S\phi_S^{n+1} + b \tag{14}$$

a_P is the coefficient of the control volume centre of the cell in question, a_N and a_S are the coefficients of control volume at the north and south boundary, respectively, *b* is the source term that incorporate all terms not included in the coefficients, and the index *n* denotes time levels. These tri-diagonal sets of equations were solved with the well-known TDMA algorithm.

4 Numerical results and discussion

The results obtained by the application of the numerical method outlined above are now presented and discussed. Three rheological models were considered, Newtonian, Oldroyd-B and UCM (although special attention was given to non-Newtonian models), and the effect of elasticity on the pulsating flow was studied for E = 0.01, 0.1, 1, 10 and 100. Analytical and numerical profiles of velocity were plotted versus time and space and compared, with due attention to mesh refinement, discretization errors and convergence rates. As in Duarte *et al* [11] the values of the non-dimensional frequency ($\alpha = 4.864$) and the pressure-gradient ratio ($K_O/K_S = 2.587$) were fixed. Because of the higher frequency response expected at high E, different time steps were used for each value of E. Thus, for E = 0.01 and 0.1 we used $\Delta t = 2 \times 10^{-3}$; for E = 1 the base time-step was $\Delta t = 2 \times 10^{-2}$; for E = 10 it was $\Delta t = 2 \times 10^{-4}$ and for E = 100 the time step used was $\Delta t = 2 \times 10^{-5}$. A good match between numerical results and analytical solutions was not found in some situations and to improve that six different computational meshes were employed 100, 200, 400, 800, 1000 and 2000 uniform control volume, i.e., with mesh spacings Δy = 0.02, 0.01, 0.005, 0.0025, 0.002 and 0.001 (for a domain spacings from $y = -1$ to $y = +1$). The discretization errors were calculated after carrying out simulations for a number of periods using different time steps and meshes until a fully established oscillatory regime was reached, i.e., with repetition at every cycle.

4.1 Start-up of the pulsating motion

The evolution of the centreline velocity of planar Poiseuille flow subjected to an oscillatory pressure gradient of a Newtonian fluid is showen in Fig.1. Starting from the situation of fluid at rest a fully-established regime is attained at approximately $t = 10$ a somewhat higher value than that acquired for start-up [11].

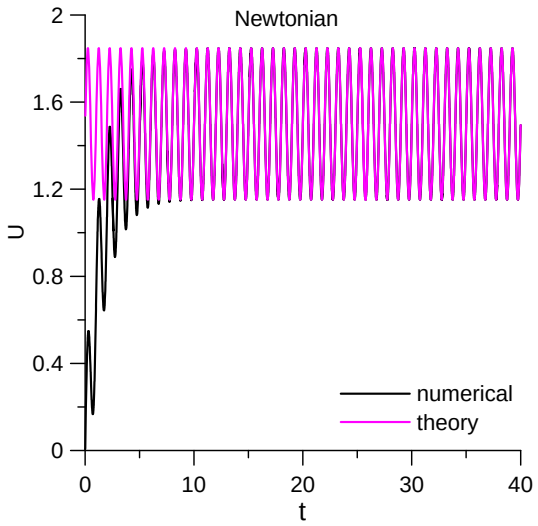

Fig.1. Evolution with time of centreline velocity during pulsating flow of Newtonian fluid at starting time.

On the other hand, the time acquired for flow development of Oldroyd-B and UCM fluids is greatly influenced by elasticity number, and a fully-established state is reached at only at very high non-dimensional time. This behaviour is illustrated in Fig.2 where the evolution of the centreline velocity for Oldroyd-B with $\beta = 0.01$ and UCM is plotted against time. Looking at these results it can be seen that the amplitude and frequency of startup-related oscillations significantly increase with elasticity (Fig.2 a) and b)). Comparing fluid models with $\beta = 0.01$ and 0, Fig.2 b) shows that decreasing β induces velocity oscillations having larger amplitudes. These lower frequency oscillations are originated by a shear wave front that oscillates from wall to wall across the channel during inception of flow which are those with origin from the sinusoidal pressure gradient.

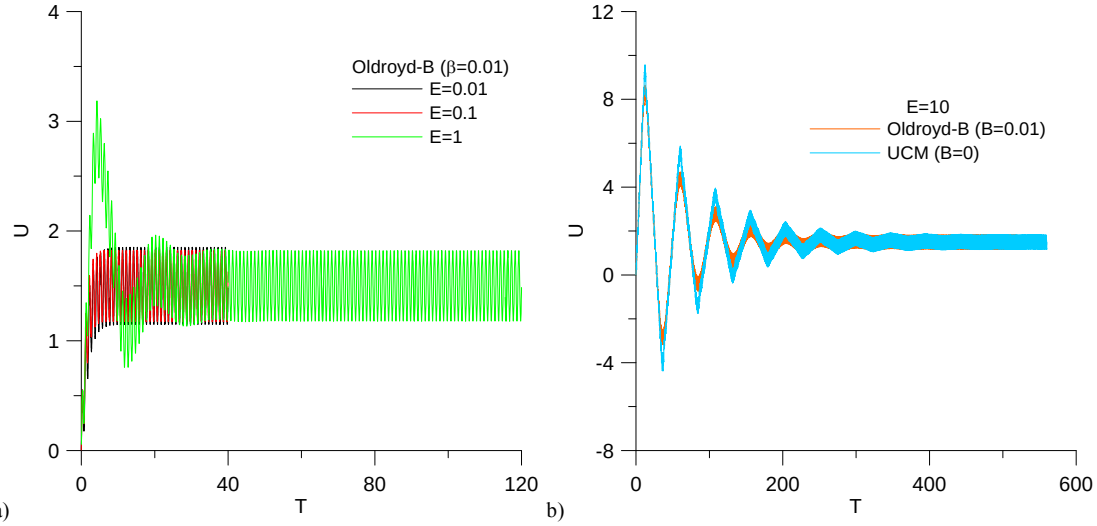

Fig.2. Evolution with time of centreline velocity during pulsating flow: a) for Oldroyd-B ($\beta = 0.01$) at different elasticity numbers (E = 0.01, 0.1 and 1); b) for Oldroyd-B ($\beta = 0.01$) and UCM ($\beta = 0$) at E = 10.

4.2 The Centerline velocity variation

From now on the numerical results are for fully-established flow conditions obtained after running the simulations for many cycles and making sure that repetition between cycles has been achieved. The evolution of the centreline velocity during one cycle using the different fluid models at E = 0.01, 0.1, 1, 10 and 100 is presented in Fig.3, from where a comparison between fluid models and analytical and numerical results can be made. From each group of figures it can be observed that, depending on the elasticity number, the behaviour of the fluids is different. Thus, at E = 0.01 (Fig.3 a)) all fluids present practically the same behaviour and good agreement between numerical results and analytical solutions was obtained even using coarse mesh $\Delta y = 1 \times 10^{-2}$. But when the elasticity is increased from 0.01 to 0.1 (Fig.3 b)), differences between fluids start to be evident.

Here, differences in phase and in the maximum velocity oscillation, can be distinguished for the UCM and Oldroyd-B fluids, with all the Oldroyd-B fluids presenting similar evolution. Like showen by Duarte *et al* [11], at E = 1 (Fig.3 c)) Oldroyd-B ($\beta > 0.005$) fluids present similar behaviour which differs significantly in amplitude and phase from that of UCM and Oldroyd-B ($\beta < 0.005$) and only in phase from Oldroyd-B ($\beta = 0.005$) fluid. Here, good agreement between numerical and analytical results was obtained for $\beta \geq 0.005$ using mesh with spacings $\Delta y = 1 \times 10^{-2}$, but for $\beta < 0.005$ was only obtained when fine meshes were used $\Delta y = 1 \times 10^{-3}$. However, at E = 10 (Fig.3 d)) all fluids with $\beta \geq 0.001$ present similar behaviour. In contrast, the velocity evolution of UCM fluid is now significantly different in amplitude, with a considerable decrease, and phase from that shown by the other fluids. Looking now at the graphic for E = 100 (Fig.3 e)) the evolution of the centreline velocity of UCM fluid increase in amplitude, being higher than for the other fluids. At E = 10 and 100 good match was obtained between analytical and numerical results for fluids with $\beta > 0$ using coarse mesh ($\Delta y = 1 \times 10^{-2}$), but in order to achieve agreement for $\beta = 0$ smaller spacing was employed.

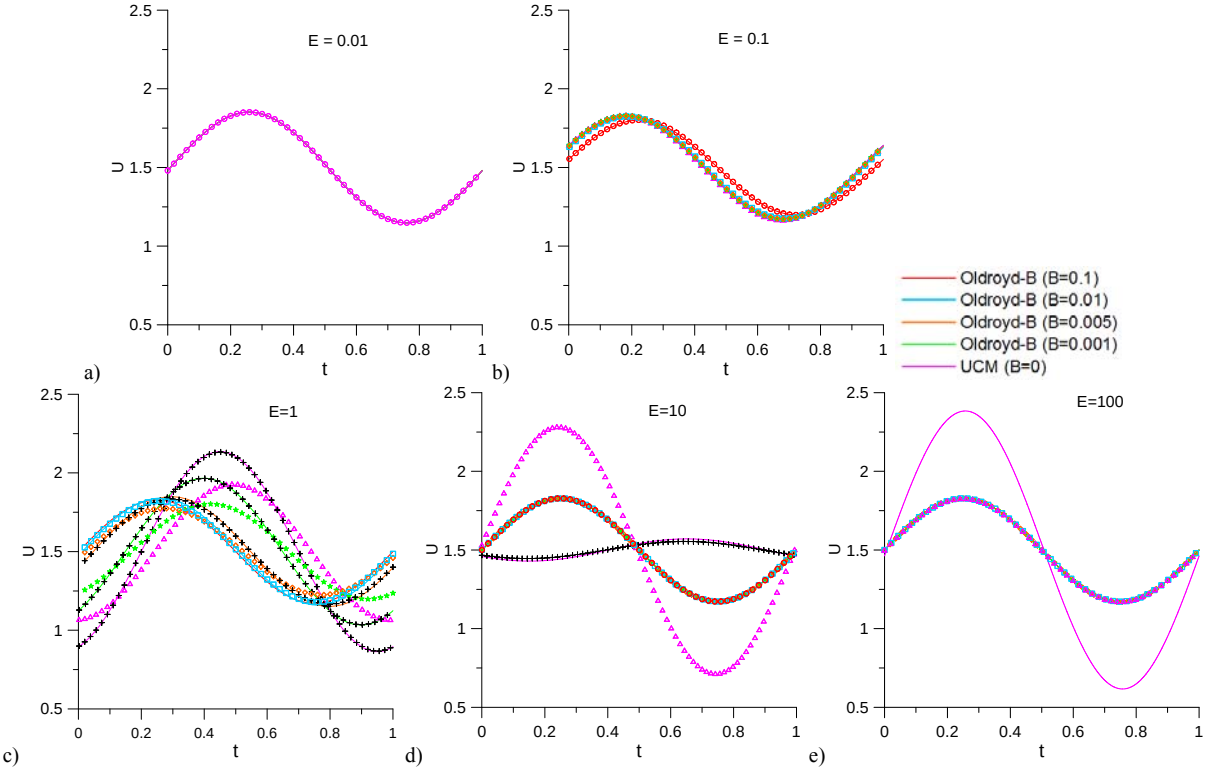

Fig.3. Analytical (lines) and numerical (symbols) results of the evolution of centreline velocity with time for the pulsating flow of various fluids: Oldroyd-B ($\beta = 0.1, 0.01, 0.005, 0.001$) and UCM ($\beta = 0$). Influence of β for various elasticity numbers: E = 0.01 a); 0.1 b); 1 c); 10 d) and 100 e). Numerical predictions with $\Delta y = 1 \times 10^{-2}$ (coloured symbol) and $\Delta y = 1 \times 10^{-3}$ (black cross).

Fig 4 shows again the evolution of centreline velocity but with the purpose of assessing the effect of elasticity for each type of fluid during one period oscillation. For viscoelastic fluids, as the solvent viscosity ratio is reduced the effect of elasticity starts to be visible. Thus, as a consequence of increasing elasticity there was first a small difference in phase at E = 0.1 when $\beta = 0.1$ (Fig.4 a)) and this difference increase for the fluid with $\beta = 0.01$ (Fig.4 b)). The Oldroyd-B ($\beta = 0.005$), illustrated in Fig.4 c), shows three different evolutions at E=0.01, 10 and 100 which present the same behaviour, 0.1 and 1. These evolutions differ from each other only in phase. However, for $\beta = 0.001$ (Fig.4 d)) the main difference is the augment in amplitude of oscillation at E = 1. Finally, looking to UCM fluid (Fig.4 e)), although, the centreline velocity at E = 0.01, 0.1 and 1 are practically the same at E = 10 and 100 shows a significant reduction and augment respectively in oscillations amplitude.

4.3 Spatial profiles and comparison with theory

Illustrative velocity profiles are presented in Fig. 5 showing how that the velocity across the channel is affected by elasticity. Those profiles were obtained at four different time instants during an oscillatory period, with phase angles ωt = 0º, 90º, 180º and 270º, for an Oldroyd-B fluid with β = 0.001. This fluid reveal, an initial increase and then a reduction of the oscillations as the elasticity number is increased from 0.01 to 100, presenting higher oscillations at E = 1. In Fig.5 a) the velocity profiles at E = 0.01 shows no oscillations much like the Newtonian case [11]. When elasticity number is increased to 0.1 (Fig.5 b)) smooth oscillations appear and at E = 1 (Fig.5 c)) the propagation of oscillating motions are clearly spread out across the channel with higher amplitude and frequency. At E = 10 (Fig.5 d)) these oscillations are no longer formed across the channel width but are restricted to a zone near the wall. This general behaviour was also observed for models with solvent viscosity ratio, β, higher than 0.001. In addition the figure clearly demonstrates that much finer meshes are required at moderate and high elasticity numbers (E = 1 and 10) in order to faithfully represent the theoretical profiles: while 50 cells across the channel are sufficient at E = 0.01 and 0.1, as many as 1000 cells are needed at E = 1.

We look now into the effect of E at constant β: Fig.6 shows velocity profiles at t = 0 for the various fluids with β varying from 1 (Newtonian) to 0 (UCM). Generally, as viscoelasticity is enhanced through added polymer concentration, i.e., when $\beta \neq 1$, the influence the influence of elasticity number becomes more pronounced. The absence of oscillations at E = 0.01 and the presence of very smooth oscillations at E = 0.1 is a general behaviour among these viscoelastic fluid models. The velocity profiles of Oldroyd-B (β = 0.1), (Fig.6 a)) at E = 1, 10 and 100 are practically equal and present smooth oscillations. Looking at the Oldroyd-B (β = 0.01) plot (Fig.6 b)) at E = 1, the velocity profile shows higher oscillations, in terms of both amplitude and frequency, than for other values of E, and at E = 10 and 100 small oscillations appear near the wall. As β is further reduced in Oldroyd-B fluid models, to β = 0.005 and 0.001, Fig.6 c) and d) respectively, oscillations at E = 1 increase in amplitude and at E = 10 and 100 the oscillations near the wall are now spread out to a higher distance from the channel wall. Finally, considering UCM fluid (Fig.6 e)) the velocity profile at E = 0.01 and 0.1 is very similar to that predicted for the other viscoelastic fluids, at E = 1 oscillations increase in amplitude and at E = 10 and 100 oscillations, previously near the wall, are completely spread out across the channel increasing significantly their frequency, although with much smaller amplitudes.

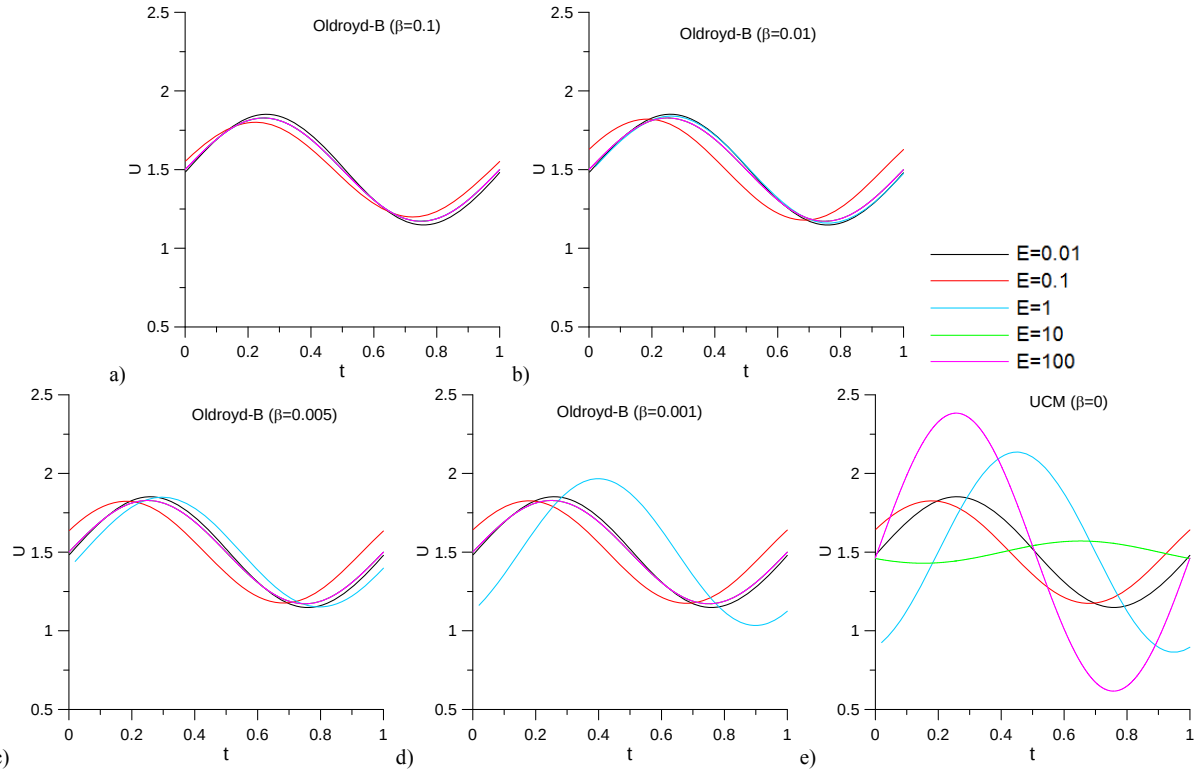

Fig.4. Evolution of centreline velocity with time during the pulsating flow of: a) - d) Oldroyd-B (β = 0.1, 0.01, 0.005 and 0.001); and f) UCM (β = 0) fluids on mesh $\Delta y = 2 \times 10^{-2}$, at E = 0.01 ($\Delta t = 2 \times 10^{-3}$), E = 0.1 ($\Delta t = 2 \times 10^{-3}$), E = 1 ($\Delta t = 2 \times 10^{-2}$), E = 10 ($\Delta t = 2 \times 10^{-4}$) and E = 100 ($\Delta t = 2 \times 10^{-5}$).

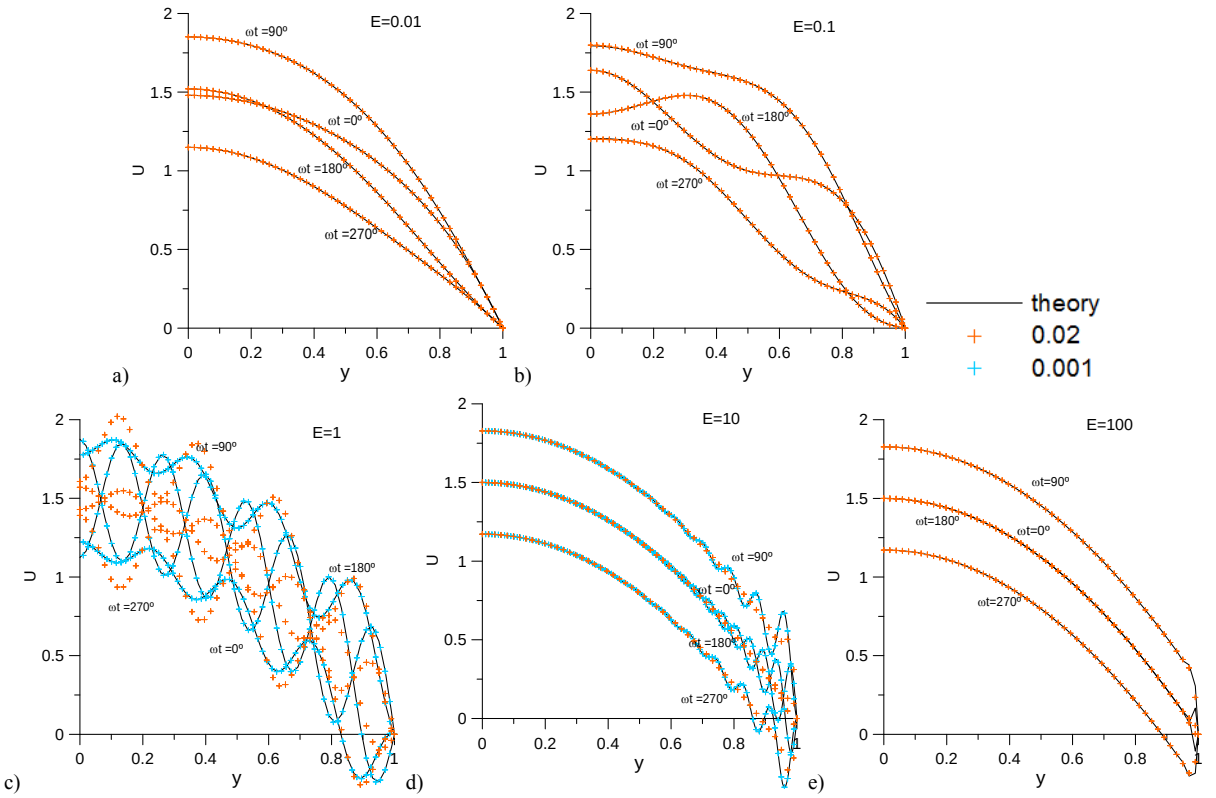

Fig.5. Numerical (symbols) and analytical (lines) results for the velocity profiles of Oldroyd-B fluid ($\beta = 0.001$) in the oscillatory regime during one cycle on meshes $\Delta y = 2 \times 10^{-2}$ and 1×10^{-2} at: a) E = 0.01 ($\Delta t = 2 \times 10^{-3}$); b) E = 0.1 ($\Delta t = 2 \times 10^{-3}$); c) E = 1 ($\Delta t = 2 \times 10^{-2}$); d) E = 10 ($\Delta t = 2 \times 10^{-4}$); e) E = 100 ($\Delta t = 2 \times 10^{-5}$). Numerical results were predicted using mesh spacings of $\Delta y = 2 \times 10^{-2}$ (orange) and $\Delta y = 1 \times 10^{-3}$ (blue).

4.4 Discretization error and convergence

Fig.7 illustrates the distribution of the discretization error along one cycle, calculated on five different uniform meshes and with corresponding smaller time steps. Here we only present the Oldroyd-B ($\beta = 0.001$) case at different values of elasticity. At the lowest value of elasticity (Fig.7a)) the error is almost a straight line with smooth oscillations and the successive refinements revealing a regular parallelism, with a constant separation as mesh spacings are decreased as $\Delta y_1 = \Delta y_2/2$, which is usual in accurate second order methods. But, when elasticity number is increased to 0.1 and 1 (Fig.7 b) and c)) it seems to follow instead a sinusoidal-like variation. Although, at E =0.1 there is a good parallelism between mesh refinements, at E = 1 a phase lag is present especially for the coarser meshes. However, if elasticity number is increased to 10 (Fig.7 d)) the error will present once again a straight-like variation. It is also important to note that the magnitude of the error increase with elasticity number. In addition, while at E = 0.01 the error is smaller than 10^{-3} at E = 10 the error is only smaller than 10^{-3} when mesh spacing $\Delta y = 1 \times 10^{-3}$.

An overall error measure was then calculated as the average error over one cycle, following Eq (12b). The corresponding convergence rates obtained for the different models at different values of elasticity over a period are illustrated in Fig.8 as symbols and the lines graphic fittings using a power-law equation $e = C10^{p\Delta y}$. In general, the size of the error increases as the elasticity number is increased until E =1, and then decrease in magnitude when E is further raised 10, but only for fluids with $\beta > 0$. Looking to each value of elasticity in particular, at E = 0.01 (Fig.8 a)) the convergence rates obtained were almost the same for all fluid cases giving a convergence rate of p = 2.01. When E is raised, the error decay lines for each value of β become separated, with consistent larger errors for smaller β. However the decay rate remains close to 2 for all cases in agreement with the 2nd order of the method.

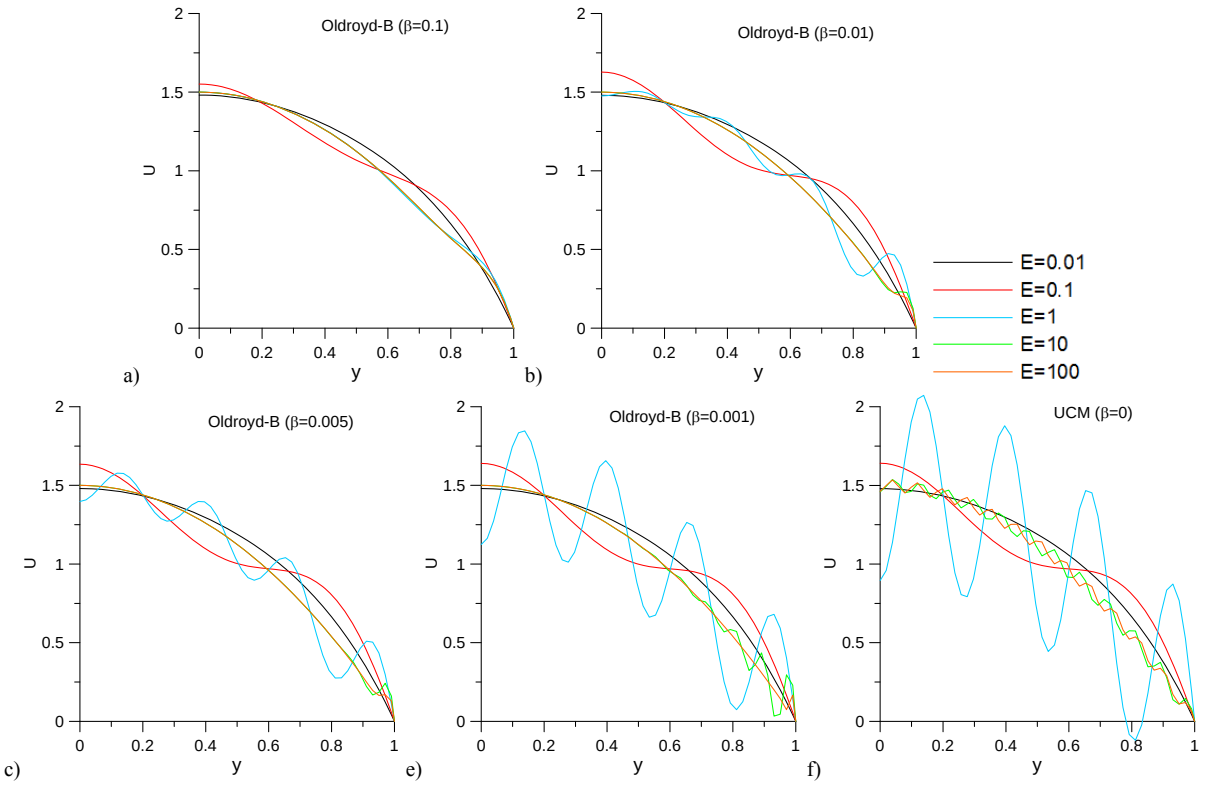

Fig.6. Velocity profiles at ωt = 0º in the oscillatory regime of: a)-d) Oldroyd-B (β = 0.1, 0.01, 0.005 and 0.001) and e) UCM (β = 0) fluids on mesh $\Delta y = 1 \times 10^{-3}$, at different values of elasticity number: E = 0.01 ($\Delta t = 2 \times 10^{-3}$), E = 0.1 ($\Delta t = 2 \times 10^{-3}$), E = 1 ($\Delta t = 2 \times 10^{-2}$), E = 10 ($\Delta t = 2 \times 10^{-4}$) and E = 100 ($\Delta t = 2 \times 10^{-5}$).

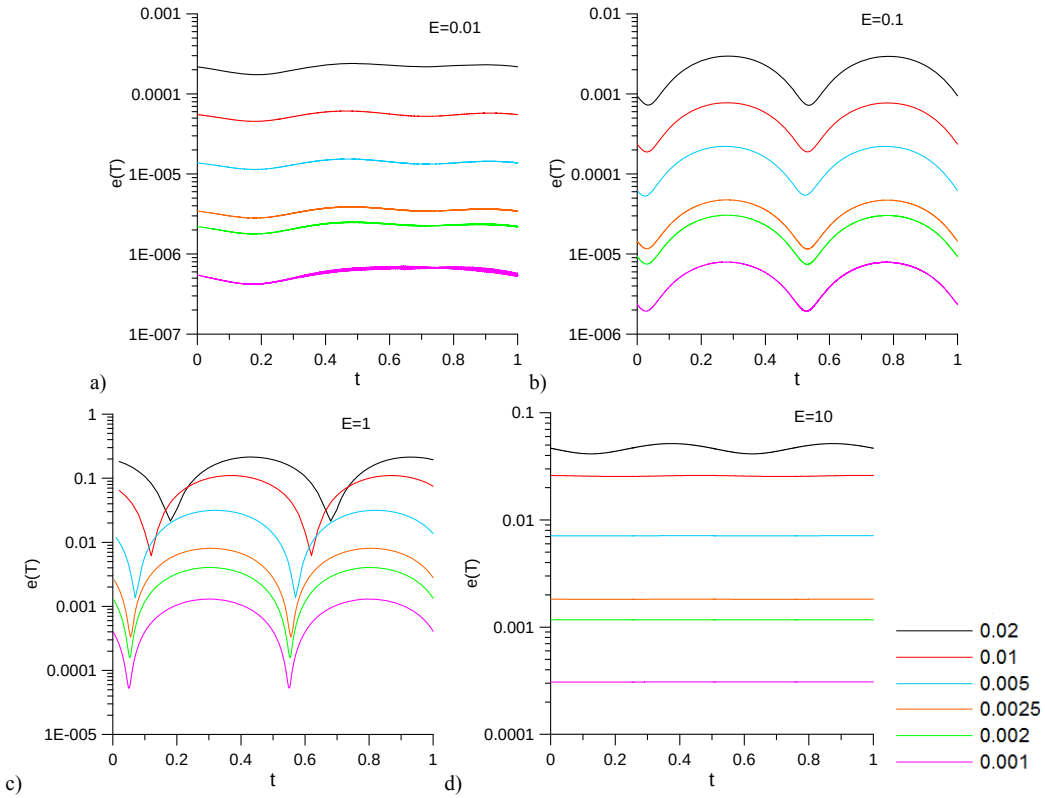

Fig.7. Evolution of the discretization error during one cycle for pulsating flow of the Oldroyd-B fluid with β = 0.001 calculated with various discretizations and elasticity numbers.

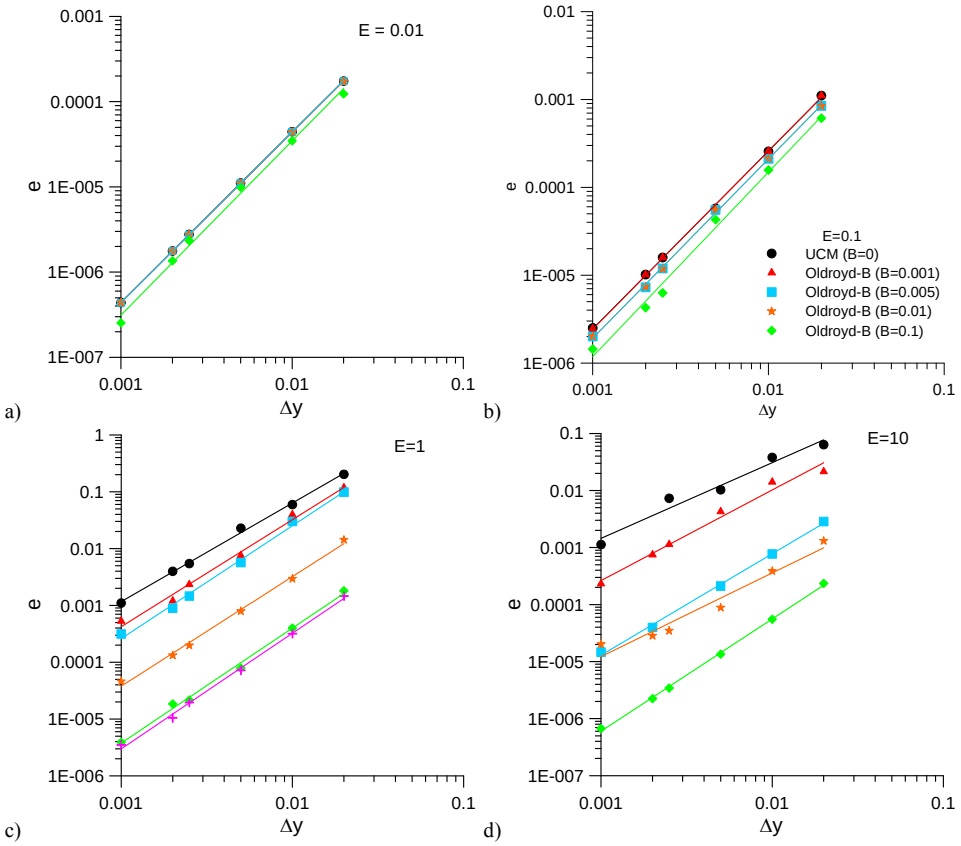

Fig.8. Convergence plots for pulsating flow of Oldroyd-B and UCM models at different values of elasticity number.

5 Conclusions

The pulsating flow problem of Duarte *et al* [11] is extended here to various values of the elasticity number.

The viscoelastic fluid flow analysis began with the evaluation of the flow during the transient regime until steady state was reached. Here it was clear that as the elasticity number was increased more time was needed to reach a fully-established pulsating regime and oscillations with longer wavelength than that imposed by the oscillating pressure gradient started to appear and significantly increase in amplitude and frequency. It was also shown that as β tends to zero the oscillations of the long wave propagation also increase in frequency and amplitude. Then, the influence of β and E was analysed during one period by looking into the centreline velocity evolution. At E = 1 the behaviour of all Oldroyd-B fluids having different β could be well distinguished, but at E <1 all fluids presented almost the same evolution and at E > 1 only the UCM fluid showed a different evolution. Also, fluids with $\beta < 0.01$ are not significantly affected by E, however as β tends to zero the value of E starts being important. Velocity profiles were also presented in a half the channel with at four different moments in time and at various values of elasticity. It was observed that as the elasticity number increases form 0.01 to 1 transverse oscillations start to develop steeper in terms of oscillation amplitude at E = 1. But as E was further increased to E = 10, oscillations were present only near the wall. In agreement with [11] it was found that as elasticity number is increased and β decreased the accuracy of numerical results deteriorate, so more refined meshes were needed to increase the accuracy.

References

1. G. Pntrelli, Pulsating blood flow in a pipe, *Computers and Fluids*, 27 (3): 367-380, 1998.
2. M. Massoudi, T. X. Phuoc, Pulsatile flow of blood using a modified second-grade fluid model, *Computers and Mathematics with Applications*, 56: 199–211, 2008.
3. X. Wang, N. Zhang, Numerical analysis of heat transfer in pulsating turbulent flow in a pipe, *International Journal of Heat and Mass Transfer*, 48: 3957–3970, 2005.
4. N. S. Deshpande, M. Barigou, Vibrational Flow of non-Newtonian Fluids, *Chemical Engineering Science*, 56: 3845–3853, 2001.

5. G. Mompean, M. Deville, Unsteady finite volume simulation of Oldroyd-B fluid through a three-dimensional planar contraction, *Journal of Non-Newtonian Fluid Mechanics*, 72: 253-279, 1997.
6. T. Manos, G. Marinakis, S. Tsangaris , Oscillating viscoelastic flow in a curved duct—Exact analytical and numerical solution, Journal of Non-Newtonian Fluid Mechanics, 135: 8–15, 2006.
7. N. Fiétier, M. O. Deville, Time-dependent algorithms for the simulation of viscoelastic flows with spectral element methods: applications and stability, *Journal of Computational Physics*, 186: 93–121, 2003.
8. M.F. Tomé, M.S.B. de Araujo, M.A. Alves, F.T. Pinho, Numerical simulation of viscoelastic flows using integral constitutive equations: A finite difference approach, *Journal of Computational Physics*, 227: 4207–4243, 2008.
9. O.G. Harlen, J.M. Rallison,, P. Szabo, A split Lagrangian-Eulerian method for simulating transient viscoelastic flows, *Journal of Non-Newtonian Fluid Mechanics*, 60: 81-104, 1995.
10. P.J. Oliveira, F.T. Pinho, G.A. Pinto, Numerical simulation of non-linear elastic flows with a general collocated finite-volume method, *Journal of Non-Newtonian Fluid Mechanics*, 79: 1–43, 1998.
11. A.S.R. Duarte, A.I.P. Miranda, P.J. Oliveira, Numerical and analytical modeling of unsteady viscoelastic flows: The start-up and pulsating test case problems, *Journal of Non-Newtonian Fluid Mechanics*, 154: 153–169, 2008.